vortex pairs. The solid lines in Fig. 4(b) are drawn with slope $\frac{3}{2}$. Over a wide range of θ, the data agree with the lines, indicating that over that angular range the mode indeed corresponds to $m = \frac{3}{2}$. There it has a wavelength equal to $\frac{2}{3}$ the circumference, and it moves at the same speed as the $m = 3$ mode. For $0.6 \lesssim \theta/2\pi \lesssim 0.7$, the mode develops a phase anomaly and "drops back" by half a wavelength so as to be able to continue periodically around the annulus. At slightly different axial positions on the same vortex pair, we have observed the transition taking place in the range $0.5 \lesssim \theta/2\pi \lesssim 0.8$ by "jumping ahead" by half a wavelength. This transition region is stationary in the laboratory frame, possibly because of pinning by slight geometric imperfections.

We are grateful to R. J. Donnelly, K. Park, E. D. Siggia, and H. L. Swinney for helpful discussions. This work was supported in part by National Science Foundation Grant No. DMR79-23289, and by the Consejo Nacional de Ciencia Technología de México and the Escuela Superior de Física y Matemática, Comisión para el Fomento Académico y Administrativo, Instituto Politécnico Nacional, Mexico.

[1]D. Coles. J. Fluid Mech. 21, 385 (1965).
[2]M. Gorman, H. L. Swinney, and D. A. Rand, Phys. Rev. Lett. 46, 992 (1981).
[3]D. A. Rand, to be published.
[4]See, for instance, T. B. Benjamin and T. Mullin, Proc. Roy. Soc. London, Ser. A 377, 221 (1981).
[5]For a recent review, see R. C. DiPrima and H. L. Swinney, in *Hydrodynamic Instabilities and the Transition to Turbulence*, edited by H. L. Swinney and J. P. Gollub (Springer, Berlin, 1981).
[6]As discussed below, WVF results in a local increase of λ near the center and a local decrease of λ near the ends of the colmun. When the local λ is greater than the maximum or less than the minimum λ which is stable for TVF at a given R/R_c, a transition to a different value of p occurs.
[7]$\varphi(\omega) = -\tan^{-1}[(R_2 I_1 - R_1 I_2)/(R_1 R_2 + I_1 I_2)]$, where $R_i(\omega)$ and $I_i(\omega)$ are the real and imaginary parts of the Fourier transforms of the two signals $i = 1, 2$.

Stimulated Raman Backscatter from a Magnetically Confined Plasma Column

A. A. Offenberger, R. Fedosejevs, W. Tighe, and W. Rozmus[a]
Department of Electrical Engineering, University of Alberta, Edmonton, Alberta T6G 2G7, Canada
(Received 28 December 1981)

Stimulated Raman backscatter from long-scale-length, magnetically confined, underdense plasma has been studied for incident CO_2 laser intensities up to 2.5×10^{11} W/cm^2. Above an incident threshold of 4×10^{10} W/cm^2 the reflectivity rapidly rises to a saturated value of 0.7%. The measurements are in good agreement with a theoretical model of absolute instability which includes both collisional and Landau damping due to hot-electron production.

PACS numbers: 52.25.Ps, 52.55.Ke

Parametric instabilities in plasmas have recently been the subject of intense theoretical investigation[1-9] because of their possible effect in reducing absorption and producing superthermal particles[10] in laser-driven fusion. Stimulated Raman scattering (SRS), which involves the scattering of an electromagnetic wave from an enhanced electron plasma wave, is one such instability. Unlike stimulated Brillouin scattering (SBS), which involves an ion wave with little dispersion and therefore satisfies easy matching conditions, SRS requires a long-scale-length underdense plasma ($n < n_c/4$) in order to provide phase matching and growth for the highly dispersive electron wave. As a consequence, SRS has not been extensively studied in present-day laser-target interaction experiments in which density-gradient scale lengths, L_n, are short. For future reactor-size plasmas, however, long gradient scale lengths are expected.

A linear magnetically confined plasma, on the other hand, does offer the prospect for providing large L_n and, indeed, was used in an early experimental study[11]—wherein SRS reflectivity levels of 10^{-5} were reported. In the present study, we report spectrally and temporally resolved meas-

urements of the growth and saturation of SRS at remarkably high reflectivity levels of 0.7% and compare results with the expected behavior for an absolute instability model.

The experiments were conducted using a long-pulse, electron-beam–excited, CO_2 laser focused by means of a 1.5-m, $f/15$ mirror into a magnetically confined ($B = 63$ kG), laser-heated, hydrogen plasma column. An astigmatic focal distribution produced by distorting one of the beam steering mirrors gave a peak intensity of 2.4×10^{11} W/cm^2 for a 1-GW input power and total measured focal depth between 90% and 50% intensity points of 28 and 85 mm, respectively. Details of the formation and heating of the plasma and generation of strong SBS have been previously reported.[12-13] The plasma density measured interferometrically at an axial distance of 4 cm from the focus varied from $\leq 0.1n_c$ at early time to an asymptotic value of $\leq 0.03n_c$ for $t > 200$ ns. By this time the plasma in the focal region had approached an asymptotic convective flow along the magnetic field lines with $L_n \simeq 40$ cm (determined by the field). The average temperature $T_e = T_i$ was 45 eV as determined from energy balance and SBS spectral measurements and was consistent with time-averaged x-ray measurements which indicated $T_e < 60$ eV. The Doppler-shifted, backscattered SBS was sufficient to modulate the tail of the laser pulse and produce groups of ~5-ns-duration spikes of up to 1-GW power (see Fig. 1); this proved crucial for inducing SRS. The groups of pulses were separated by the laser-plasma round-trip time, ~160 ns, with individual pulses separated by the 22-ns unstable resonator transit time. Backscattered SBS and SRS radiation collected by the focusing mirror was temporally (1.5-ns resolution) and spectrally analyzed using various filters. A NaCl dispersing prism and pyroelectric infrared multichannel analyzer were used to give single-shot, time-integrated spectra with a resolution of 0.18 μm full width at half maximum. Reflectivity calibration was determined by using normal reflection from a polished

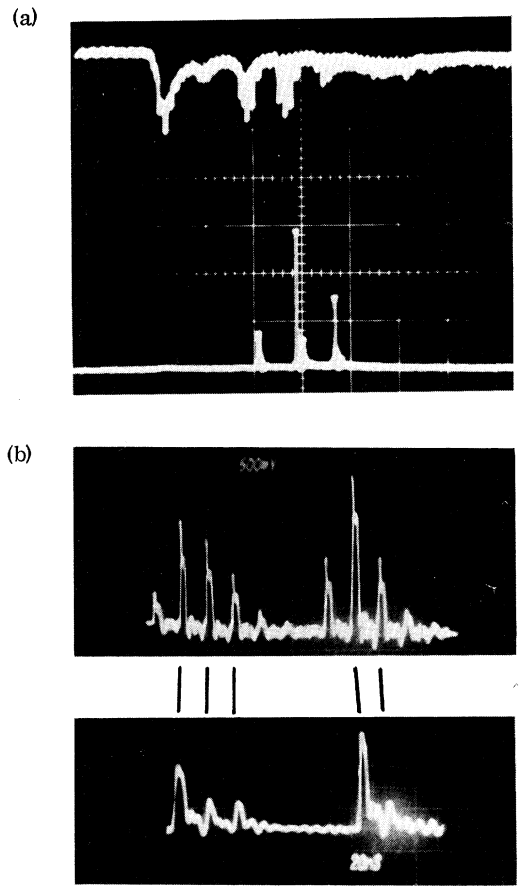

FIG. 1. Oscilloscope traces of corresponding input CO_2 (upper trace) and Raman backscatter (lower trace) pulses (a) at 200 ns/division and (b) for a different shot in the tail of the CO_2 laser pulse at 20 ns/small division.

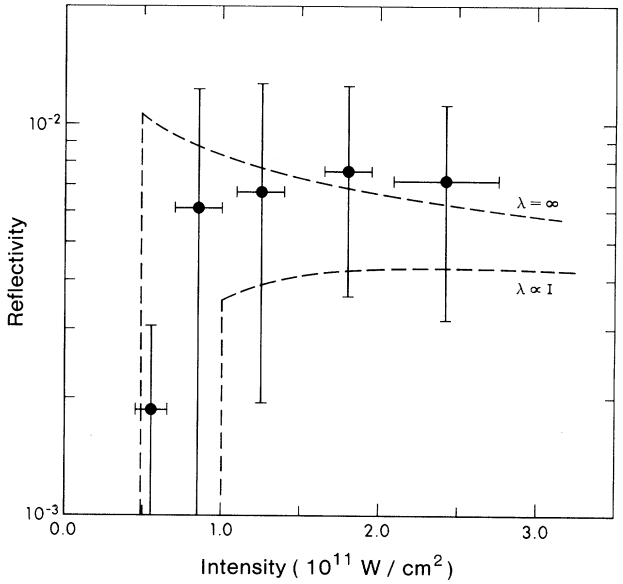

FIG. 2. Raman reflectivity as a function of incident intensity. The circles represent the average measured reflectivities from numerous laser shots with error bars showing the standard deviation for each averaged set of data. The lines represent theoretical curves for a saturated finite inhomogeneous absolute instability: upper curve for $\lambda = \infty$ and lower curve for $\lambda = (9.83 \times 10^{-12}\ \text{cm}^2/\text{W})I$.

NaCl flat.

Raman backscatter was observed as a series of ~5-ns-duration spikes which coincided with the high-intensity spikes in the tail of the CO_2 laser pulse (Fig. 1). In contrast to the strong SBS signal which appeared promptly with plasma formation,[13] no SRS was observed until ~400 ns after gas breakdown. There was no direct correlation between the strongest Raman and strongest Brillouin pulses and, in addition, the Brillouin pulses were much shorter, ≤ 3 ns in duration. The first pulse within each CO_2 laser pulse group produced little SRS, which can be explained by the large electron collisional damping in the cold plasma remaining after the preceding period of reduced heating (the estimated thermal relaxation time was ~30 ns). The second and third pulses in each group, on the other hand, consistently produced Raman backscatter (dependent on CO_2 intensity) but even for these pulses varying plasma conditions led to considerable scatter in reflectivity. The average reflectivity, R, obtained from these second and third pulses is plotted as a function of incident intensity in Fig. 2. A threshold of 4×10^{10} W/cm^2 was observed below which $R<10^{-4}$. Error bars represent standard deviations of the average points and an additional estimated limit for systematic error of ± 30% should be included in both reflectivity and intensity.

Typical single-shot, time-integrated spectral measurements are shown in Fig. 3. When there was predominantly one backscatter pulse, a single spectral peak was observed [Fig. 3(a)] with spectral widths varying from less than resolution limited, 0.18 μm, to 0.5 μm. Most shots involving multiple backscatter pulses showed structured spectra, probably resulting from integration of a number of pulses with slightly different density conditions. The average reflected wavelength was 12.7 μm corresponding to an electron density $n_e = 2.7\times10^{17}$ cm^{-3}, but during the course of many measurements spectral structure was observed over the range of 12.0 to 13.5 μm for which n_e varied from 1.5 to 4.5×10^{17} cm^{-3}.

The Raman backscatter process is a parametric instability involving an electromagnetic pump wave (designated 1), a backscattered electromagnetic (em) wave (2), and an electron plasma wave (3) satisfying the dispersion relations $\omega_{1,2}^2 = \omega_{pe}^2 + c^2k_{1,2}^2$ and $\omega_3^2 = \omega_{pe}^2 + 3v_e^2k_3^2$, respectively, where $\omega_{pe}^2 = 4\pi n_e e^2/m_e$ and $v_e^2 = T_e/m_e$. For an inhomogeneous system of finite extent[4,5,9] or in the presence of sufficiently strong incoherent

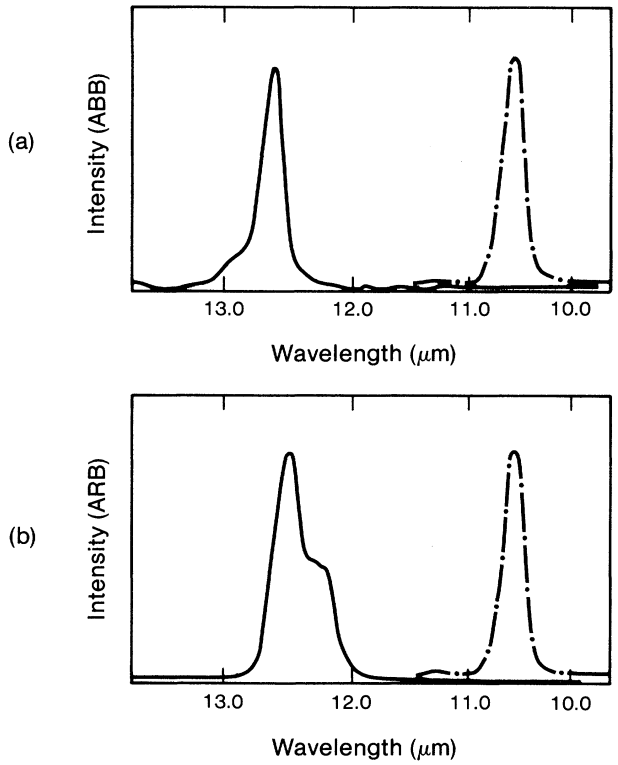

FIG. 3. Raman backscatter spectra (solid lines) and CO_2 input reference spectra (dashed lines) (a) for the case of predominantly a single backscatter spike; (b) for the laser shot shown in Fig. 1(a).

fluctuations[6,7] it has been shown that absolute instability is possible. In the present case, the limited depth of focus and residual density fluctuations arising from the damped SBS could both possibly contribute to onset of such an absolute instability. For a finite system an approximate SRS growth rate is given by[4]

$$\gamma_{gr} = [2\gamma_0(v_2v_3)^{-1/2}(1-\pi^{-1/2}\lambda^{-2/3}) - (\gamma_2/v_2+\gamma_3/v_3)](v_2v_3)/(v_2+v_3),$$

where $\gamma_0 = k_3v_0[\omega_{pe}/(\omega_1-\omega_{pe})]^{1/2}/2\sqrt{2}$ is the homogeneous growth rate, $v_0 = e(4\pi I_1/c)^{1/2}/m_e\omega_1$, I_1 is the intensity of the circularly polarized incident wave, $\lambda = \gamma_0^2/(\kappa' v_2v_3)$, $\kappa' = d(k_1+k_2-k_3)/dx$ is the phase mismatch gradient, and v_i and γ_i ($i=1$, 2,3) are the group velocities and damping rates for the three waves. The equation for γ_{gr} was derived under the assumption that $\lambda \gg 1$, and κ' = const. In the present case the em wave is weakly damped giving $\gamma_3/v_3 \gg \gamma_2/v_2$. Evidently, for absolute instability both inhomogeneity ($\lambda > \pi^{-0.75}$) and damping [$\gamma_3 < \gamma_0(v_3/v_2)^{1/2}$] criteria must be satisfied.

We now analyze our experimental results in the light of our known plasma conditions. We first note that from spectral measurements the typical density $n_e = 2.7\times10^{17}$ cm^{-3} agrees with the late-time interferometric value. Consider now the *threshold* conditions. The inhomogeneity criterion can be expressed as $v_0^2/c^2 > 1.7k_0/k^2L_n$ which gives a threshold $I_{th}\sim5\times10^{10}$ W/cm^2 for $L_n = 40$ cm. This value agrees very well with experiment and, moreover, accounts for the delay for threshold to be achieved through plasma expansion generating a large enough L_n. It may also be noted that the observed spectral width of <0.8 μm (resolution limited) corresponds to a density variation $|\pm\Delta n_e/n_e| < 0.06$ which for a focal interaction length of 28 mm implies a lower bound for L_n of 23 cm.

The second criterion is set by the damping threshold. In order to determine the collisional wave damping (γ_{ei}) we need to calculate the transient electron heating. During the laser spike, $\tau_p = 5$ ns, the electrons in the focal region do not have time to cool or transfer their energy to ions and thus the electron temperature is given by simple energy balance through inverse bremsstrahlung heating, $T_e = [2k_\nu I\tau_p/3n_e + T_{e0}^{2.5}]^{0.4}$, where $k_\nu(\mathrm{cm}^{-1}) = 10^{-35}n_e^2\ln\Lambda(\omega)$ is the absorption coefficient, $\ln\Lambda(\omega) = 6.7$ is the frequency-dependent Coulomb logarithm, and $T_{e0} = 45$ eV. With T_e determined (80–130 eV over the intensity range of interest), the collisional damping, $\gamma_{ei}(\mathrm{s}^{-1}) = 3\times10^{-6}n_e\ln\Lambda T_e^{-3/2}$, where $\ln\Lambda = 9$ is the collisional Coulomb logarithm, can be evaluated. With these results it is straightforward to show that the self-consistent damping threshold intensity is 4.4×10^{10} W/cm^2. Thus simple plasma heating and expansion appear to be sufficient to achieve SRS threshold at a value of $(4-5)\times10^{10}$ W/cm^2.

We now consider a possible model for *saturation* of the instability. One may reasonably expect nonlinear mechanisms (e.g., wave breaking) to produce hot electrons. It has been observed in numerical simulation[10] that Raman scattering produces an approximately Maxwellian temperature $T_h = \frac{1}{2}mv_{ph}^2$ where $v_{ph} = \omega_3/k_3$. The additional Landau damping due to these hot electrons can be calculated giving

$$\gamma_{lh} = \left(\frac{\pi}{8}\right)^{1/2}\frac{\omega_3}{(k_3\Lambda_D)^3}\frac{n_h}{n_e}\left(\frac{T_e}{T_h}\right)^{3/2} \times\exp\left[-\frac{T_e}{2(k_3\lambda_D)^2T_h}-\frac{3T_e}{2T_h}\right],$$

where n_h, n_e, T_h, and T_e are the hot and cold densities and temperatures, respectively, and $\lambda_D = v_e/\omega_p$ is the cold-electron Debye length. For the conditions of the present experiment, $k_3\lambda_D < 0.18$, Landau damping from cold electrons is negligible and the hot-electron Landau damping ($T_h = 2.1$ keV) reduces to $\gamma_{lh}^{-1} = (6.8\times10^{-5}$ cm^3 s$^{-1})n_h^{-3}$. The density of hot electrons can be estimated from an energy flux balance[10] modified to allow for the fraction of energy dissipated by collisions giving $n_h = 2\sqrt{2}\omega_3\gamma_{lh}RI/m_ev_{ph}^3\omega_2\gamma_3$ where the total damping is $\gamma_3 = \gamma_{ei} + \gamma_{lh}$. Thus above threshold a self-consistent saturation reflectivity (for which $\gamma_{gr} = 0$) can be calculated by taking into account the additional damping due to hot electrons. These saturated reflectivities are plotted in Fig. 2 for two cases: $\lambda = \infty$, which ignores the effect of the density gradient, and $\lambda = (9.8\times10^{-12}$ cm^2/W$)I_1$, which corresponds to experimental conditions but ignores the restriction $\lambda \gg 1$ used to derive γ_{gr}. Taking these two curves as limiting cases between which the real reflectivity should lie, we see that the predicted dependence of reflectivity on intensity agrees remarkably well with the experimental measurements. At best such an analysis is still imcomplete since no account was taken of the nonuniformity of κ' in a real density gradient or the effect of density fluctuations $\delta n/n \geq 0.01$ driven by the large levels of SBS and SRS. The finite interaction length (limited by depth of focus) and nonlinearity of κ' makes the infinite inhomogeneous convective model of Rosenbluth, White, and Liu[2] inapplicable to the present experiment.

The above model would predict hot-electron densities of $\sim3\times10^{14}$ cm^{-3} and fluctuation levels[3] $\delta n_e/n_e \lesssim 0.02$ for $I < 2\times10^{11}$ W/cm^2 and maximum Landau damping. An attempt to measure x rays generated by these hot electrons was inconclusive since the low level of emission limited detectability to an estimated density of $n_h\sim2\times10^{14}$ cm^{-3}. For the estimated fluctuation level other nonlinear damping mechanisms, such as electron trapping, are not expected to be significant.

In conclusion, clear measurements have been obtained of the spectral, temporal, and saturation features of Raman backscatter from a long underdense plasma. The observed threshold and saturation show good agreement with an absolute instability-growth model which includes Landau damping due to production of hot electrons.

Financial support for this project through the Alberta/Canada Energy Resources Research Fund, a joint Program of the Federal and Alberta governments and administered by Alberta Energy

and Natural Resources, is gratefully acknowledged. In addition, the authors gratefully acknowledge useful discussion with T. W. Johnston and D. W. Forslund, the technical assistance of B. Arnold, and financial support from the Natural Sciences and Engineering Research Council of Canada.

[a]Permanent address: Institute for Nuclear Research, Warsaw, Poland.

[1]K. Nishikawa, J. Phys. Soc. Jpn. 24, 916 (1968).

[2]M. N. Rosenbluth, R. B. White, and C. S. Liu, Phys. Rev. Lett. 31, 1190 (1973).

[3]J. F. Drake, P. K. Kaw, Y. C. Lee, G. Schmidt, C. S. Liu, and M. N. Rosenbluth, Phys. Fluids 17, 778 (1974).

[4]D. F. Dubois, D. W. Forslund, and E. A. Williams, Phys. Rev. Lett. 33, 1013 (1974).

[5]D. Pesme, G. Laval, and R. Pellat, Phys. Rev. Lett. 31, 203 (1973).

[6]D. R. Nicholson and A. N. Kaufman, Phys. Rev. Lett. 33, 1207 (1974).

[7]G. Laval, R. Pellat, and D. Pesme, Phys. Rev. Lett. 36, 192 (1976).

[8]D. W. Forslund, J. M. Kindel, and E. L. Lindman, Phys. Fluids 18, 1002 (1975).

[9]F. W. Chambers and A. Bers, Phys. Fluids 20, 466 (1977).

[10]K. Estabrook, W. L. Kruer, and B. F. Lasinski, Phys. Rev. Lett. 45, 1399 (1980).

[11]R. G. Watt, R. D. Brooks, and Z. A. Pietrzyk, Phys. Rev. Lett. 41, 170 (1978).

[12]D. C. D. McKen, W. Tighe, R. Fedosejevs, and A. A. Offenberger, to be published.

[13]R. Fedosejevs, W. Tighe, D. C. D. McKen, and A. A. Offenberger, Opt. Commun. 40, 35 (1981).

Thermoelastic Effect in Niobium at the Superconducting Transition

D. G. Blair and J. Ferreirinho

Department of Physics, University of Western Australia, Nedlands, Western Australia 6009, Australia

(Received 13 May 1982)

An abrupt decrease in the acoustic loss Q^{-1} has been observed in flexural modes of polycrystalline Nb disk samples on cooling through the superconducting transition temperature T_c. High-resolution measurements on a 1.6-kHz mode of one sample showed a 30% decrease in Q^{-1} in a 20-mK temperature interval. It is shown that these results are clearly identifiable with the reduction of the thermoelastic contribution to the acoustic loss in the superconducting state.

PACS numbers: 62.40.+i, 65.70.+y, 74.30.Gn

Interest in the acoustic-loss mechanisms in solids at low temperatures has been stimulated by the requirement for very high mechanical Q factors in gravitational radiation antennas.[1,2] One material known to have a high Q is niobium. As a superconductor, Nb may be expected to show a decrease in Q^{-1} below T_c because of the BCS temperature dependence of the electronic contribution to Q^{-1}, which is well known from ultrasonic studies.[3] Previously reported measurements for Nb disk samples[4] showed decreased losses below T_c which appeared consistent with this interpretation.

The high-resolution measurements reported here show that the decrease is much too abrupt to be explained by the BCS electronic contribution. We show that the results are in fact the first observation of the thermoelastic effect[5] at low temperatures. In this effect, which is the thermodynamic reciprocal of thermal expansion, heat flow tends to restore thermal equilibrium between regions compressed (heated) and dilated (cooled) by the acoustic wave. The magnitude of the thermoelastic temperature gradients is determined by the coefficient of linear thermal expansion α, while the losses depend also on the thermal diffusion time τ_{th}. The reduction in thermoelastic contribution to Q^{-1} is due to the abrupt changes in α (Ref. 6) and the specific heat c (Ref. 7) on cooling through T_c.

We present results obtained from Q^{-1} measurements on the four different disk samples described in Table I. The disks were machined from polycrystalline Nb of 99.9% purity. The flexural modes for which measurements were made have the form

$$w(r, \theta) = w_0 \cos n\theta [J_n(k_{0n}r) + \beta_n I_n(k_{0n}r)] \quad (1)$$

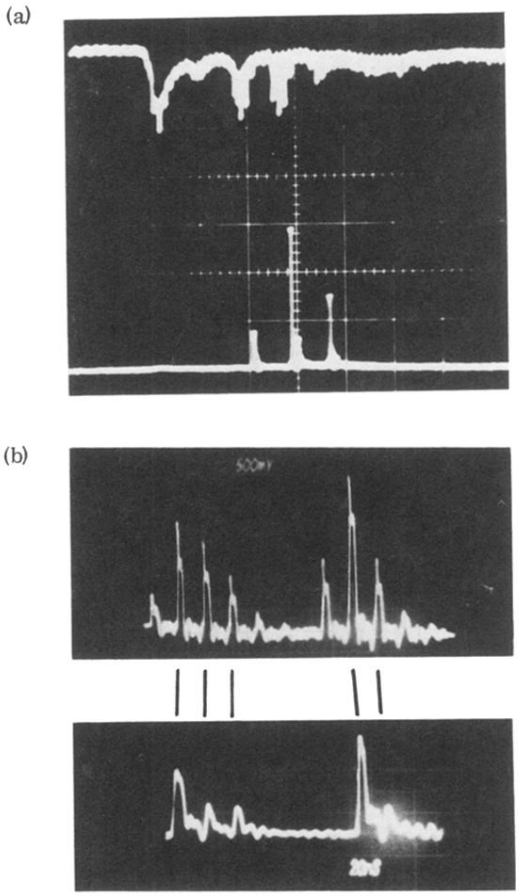

FIG. 1. Oscilloscope traces of corresponding input CO_2 (upper trace) and Raman backscatter (lower trace) pulses (a) at 200 ns/division and (b) for a different shot in the tail of the CO_2 laser pulse at 20 ns/small division.